Suppplementary Information: "Mechanical oscillation and cooling actuated by the optical gradient force"

Qiang Lin, Jessie Rosenberg, Xiaoshun Jiang, Kerry Vahala, Oskar Painter*

Thomas J. Watson, Sr., Laboratory of Applied Physics,

California Institute of Technology, Pasadena, CA 91125

(Dated: May 4, 2009)

Abstract

We present in this supporting material to our manuscript entitled, "Mechanical oscillation and cooling actuated by optical gradient forces," the detailed analysis related to estimates of the optical gradient force and effective motion mass, modeling of the optical cavity transmission and its power spectrum, simulations of optomechanical oscillation, and the effective cooling of the micro-mechanical system.

*Electronic address: opainter@caltech.edu; URL: http://copilot.caltech.edu

I. OPTICAL GRADIENT FORCE IN A DOUBLE-DISK NOMS

As the mode confinement in a double-disk NOMS is primarily provided by the transverse boundaries formed by the two disks, the double-disk structure can be well approximated by a symmetric double-slab waveguide shown in Fig. S1. For the bonding mode polarized along the $\hat{e}_y$ direction, the tangential component of the electric field is given by:

$$E_y = \begin{cases} Ae^{-\gamma x}, & x > h + x_0/2 \\ B\cos\kappa x + C\sin\kappa x, & x_0/2 < x < h + x_0/2 \\ D\cosh\gamma x, & -x_0/2 < x < x_0/2 \\ B\cos\kappa x - C\sin\kappa x, & -x_0/2 > x > -h - x_0/2 \\ Ae^{\gamma x}, & x < -h - x_0/2 \end{cases} \tag{S1}$$

where κ is the transverse component of the propagation constant inside the slabs and γ is the field decay constant in the surrounding area. They are given by the following expressions:

$$\kappa^2 = k_0^2 n_c^2 - \beta^2, \qquad \gamma^2 = \beta^2 - k_0^2 n_s^2, \tag{S2}$$

where $k_0 = \omega_0/c$ is the propagation constant in vacuum and $\beta = k_0 n_{\text{eff}}$ is the longitudinal component of the propagation constant of the bonding mode. n_{eff} is the effective refractive index for the guided mode. Accordingly, the tangential component of the magnetic field can be obtained through $H_z = \frac{-i}{\mu\omega_0}\frac{\partial E_y}{\partial x}$. The continuity of E_y and H_z across the boundaries requires κ and γ to satisfy the following equation:

$$\kappa\gamma[1 + \tanh(\gamma x_0/2)] = \left[\kappa^2 - \gamma^2 \tanh(\gamma x_0/2)\right]\tan\kappa h, \tag{S3}$$

which reduces to $\tan\kappa h = \gamma/\kappa$ when $x_0 \to 0$, as expected.

The circular geometry of the double disk forms the whispering-gallery mode, in which the resonance condition requires the longitudinal component of the propagation constant, β, to be fixed as $2\pi R\beta = 2m\pi$, where R is the mode radius and m is an integer. Thus, any variation on the disk spacing x_0 transfers to a variation on the resonance frequency ω_0 through Eqs. (S2) and (S3), indicating that ω_0 becomes a function of x_0. By using these two equations, we find that the optomechanical coupling coefficient, $g_{\text{OM}} = \frac{d\omega_0}{dx_0}$, is given by the general form

$$g_{\text{OM}}(x_0) = \frac{\frac{c\chi\gamma^2}{k_0}\text{sech}^2\left(\frac{\gamma x_0}{2}\right)}{4(n_c^2 - n_s^2)\tan\kappa h + n_s^2 x_0 \chi \text{sech}^2\left(\frac{\gamma x_0}{2}\right) + 2\xi\left[(n_c^2\gamma h\csc^2\kappa h + 2n_s^2)\tan\kappa h + \frac{n_s^2\kappa}{\gamma} - \frac{n_c^2\gamma}{\kappa}\right]} \tag{S4}$$

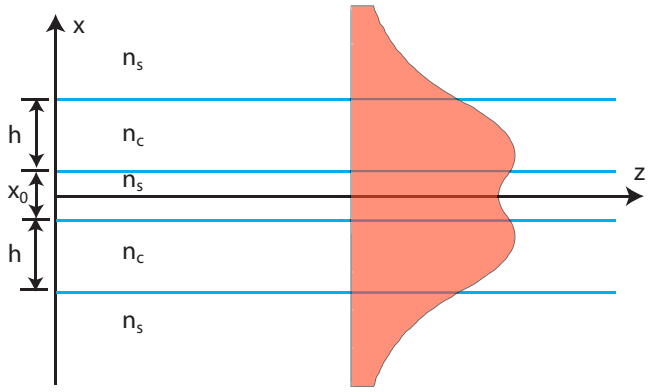

FIG. S1: Schematic of a symmetric double-slab waveguide. h and x_0 are the slab thickness and the slab spacing, respectively. n_c and n_s are the refractive indices for the slab and surrounding area, respectively.

where $\chi \equiv \kappa + \gamma \tan \kappa h$ and $\xi \equiv 1 + \tanh(\frac{\gamma x_0}{2})$.

When $x_0 \to 0$, Eq. (S4) leads to the maximum optomechanical coupling as

$$g_{\mathrm{OM}}(0) = \frac{\omega_0 \gamma^3}{2\beta^2 + 2k_0^2 n_c^2 \gamma h}. \tag{S5}$$

In analogy to Fabry-Parot cavities and microtoroids, the magnitude of the optomechanical coupling can be characterized by an effective length, L_{OM}, defined such that $g_{\mathrm{OM}} \equiv \frac{\omega_0}{L_{\mathrm{OM}}}$. Equation (S5) infers a minimum effective length

$$L_0 = \frac{2}{\gamma}\left[1 + \frac{k_0^2}{\gamma^2}(n_s^2 + n_c^2 \gamma h)\right] = \frac{\lambda_0}{\pi}\frac{n_{\mathrm{eff}}^2 + k_0 h n_c^2 \sqrt{n_{\mathrm{eff}}^2 - n_s^2}}{\left(n_{\mathrm{eff}}^2 - n_s^2\right)^{3/2}}, \tag{S6}$$

which is approximately on the order of the optical wavelength λ_0.

Physically, as the two slabs are coupled through the evanescent field between them with amplitude decaying exponentially with slab spacing at a rate γ [see Eq. (S1)], the resulting optomechanical coupling can be well approximated by an exponential function

$$g_{\mathrm{OM}}(x_0) \approx g_{\mathrm{OM}}(0) e^{-\gamma x_0}, \tag{S7}$$

where $g_{\mathrm{OM}}(0)$ is given by Eq. (S5). As indicated by the red curve in Fig. 1(g) in the main text, Eq. (S7) provides an excellent approximation for the optomechanical coupling coefficient in a double-disk NOMS. Therefore, the approximate effective length, $L_{\mathrm{OM}} \approx \frac{\omega_0}{g_{\mathrm{OM}}(0)} e^{\gamma x_0}$, agrees well with the results simulated by the finite element method [see Fig. 1(g) of the main text], and the effective length grows roughly exponentially with the disk spacing.

II. EFFECTIVE MOTIONAL MASS FOR THE FLAPPING MODE

With a clamped inner edge and a free outer edge, the mechanical displacement of a double disk exhibiting a flapping mode is generally a function of radius (Fig. S2). What matters the optomechanical effect, however, is the disk spacing at the place where the whispering-gallery mode is located, as that determines the magnitude of the splitting between the bonding and antibonding cavity modes. As the mechanical displacement actuated by the gradient force is generally small compared with the original disk spacing x_0, we can assume it is uniform in the region of the whispering-gallery mode and define the effective disk spacing $x_m(r_0)$ at the mode center, where r_0 is the radius of the whispering-gallery mode. The effective mechanical displacement is then given by $x_{\text{eff}} = x_m(r_0) - x_0$, corresponding to an effective mechanical potential energy of $E_p = m_x \Omega_m^2 x_{\text{eff}}^2/2$, where m_x is the corresponding effective motional mass and Ω_m is the resonance frequency of the flapping mode. Note that x_{eff} is twice as the real displacement at the mode center for a single disk, $x_{\text{eff}} = 2d(r_0)$. E_p reaches its maximum value when the double disk is at rest at its maximum displacement, at which point all of the mechanical energy is stored in the strain energy U_s. Therefore, $E_p = U_s$ and the effective motional mass is given by

$$m_x = \frac{2U_s}{\Omega_m^2[x_m(r_0) - x_0]^2} = \frac{U_s}{2\Omega_m^2 d^2(r_0)}, \tag{S8}$$

where both U_s and $d(r_0)$ can be obtained from the mechanical simulations by the finite element method.

The relationship between the effective mass and the physical mass of the double-disk NOMS can be found by examining the mechanical potential energy. With a mechanical displacement $d(r)$ for each single disk [Fig. S2], we can find the total mechanical potential energy by integrating over the disk regions involved in the flapping motion:

$$E_p = \int_{r_a}^{r_b} \Omega_m^2 d^2(r) \zeta 2\pi r h dr, \tag{S9}$$

where ζ is the material density, h is the thickness for a single disk, r_a and r_b are the inner and outer radii of the disk region involved in the flapping motion (see Fig. S2). Note that E_p is the total potential energy for the two disks, which is simply two times that of single one because of the symmetry between the two disks. As the physical mass of a single disk region involving in the flapping motion is given by $m_p = \pi \zeta h(r_b^2 - r_a^2)$, using Eq. (S9), we find that the effective mass is

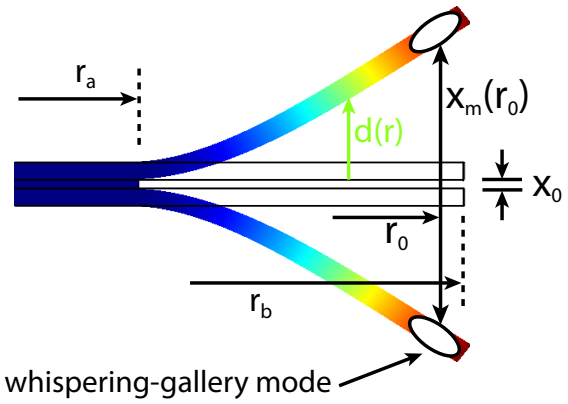

FIG. S2: Illustration of the disk displacement. x_0 is the disk spacing in the absence of the optical field. r_0 is the radius of the whispering-gallery mode. $x_m(r_0)$ corresponds to the effective disk spacing at the mode center. r_a and r_b are the inner and outer radii of the disk region involved in the flapping motion. $d(r)$ is the mechanical displacement at radius r.

related to the physical mass through the following expression:

$$m_x = \frac{4m_p}{\left(r_b^2 - r_a^2\right)\left[x_m(r_0) - x_0\right]^2}\int_{r_a}^{r_b} r d^2(r)dr = \frac{m_p}{\left(r_b^2 - r_a^2\right)d^2(r_0)}\int_{r_a}^{r_b} r d^2(r)dr. \tag{S10}$$

As the whispering-gallery mode is generally located close to the disk edge (*i.e.*, the mode radius $r_0 = 44$ μm in a double disk with $r_b = 45$ μm), $d^2(r)/d^2(r_0) \ll 1$ for most of the region between r_a and r_b, and Eq. (S10) shows that $m_x \ll m_p/2$. Therefore, the effective mass is significantly less than half the physical mass of a single disk region. In practice, the effective mass is much smaller than this value because of the real displacement function $d(r)$. For the 90-μm device used in our experiment, the effective mass is 0.264 nanogram, only about one fifth of the physical mass of a single disk region $m_p = 1.18$ nanogram. The effective mass decreases to 0.145 nanogram for the 54-μm device, due to the decrease in the disk radius.

III. LINEAR TRANSMISSION OF AN OPTOMECHANICAL CAVITY

Unlike other microcavities in which the linear transmission is determined only by the cavity loss and dispersion, for the double-disk NOMS, even the small thermal Brownian motions of the flapping mode introduce significant perturbations to the cavity resonance due to the gigantic opto-mechanical coupling, leading to considerably broadened cavity transmission. Figure S3(a) shows an example of the cavity transmission of Sample I. With a small input power of 5.8 μW

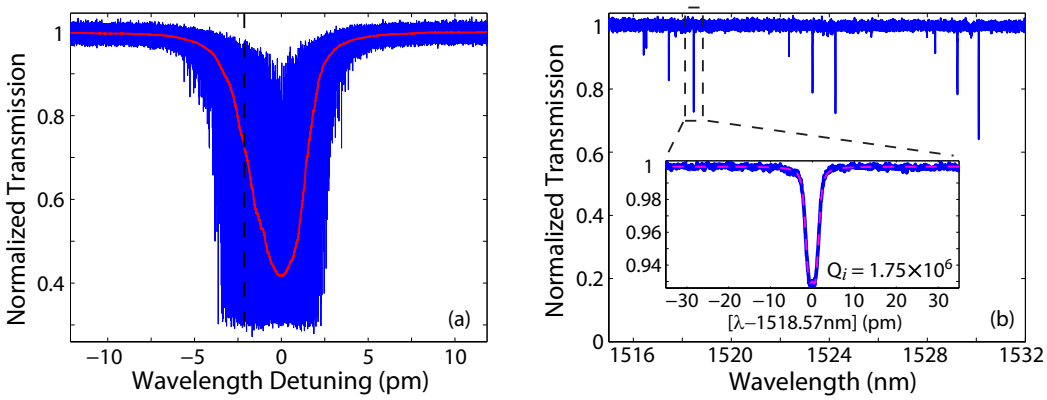

FIG. S3: (a) The cavity transmission of Sample I in a nitrogen environment, when the laser is scanned across the cavity resonance at 1518.57 nm with an input power of 5.8 μW. The blue curve is the instantaneous signal collected by the high-speed detector and the red curve is the average signal collected by the slow reference detector 2. The slight asymmetry in the transmission spectrum is due to the static component of mechanical actuation when the laser is scanned from blue to red. The dashed line indicates the laser frequency detuning used to record the power spectral density shown in the top panel of Fig. 3(b) in the main text. (b) Linear scan of the averaged cavity transmission of Sample I at an input power of 2.9 μW. The inset shows a detailed scan for the bonding mode at 1518.57nm, with the experimental data in blue and the theoretical fitting in red.

well below the oscillation threshold, the cavity transmission exhibits intense fluctuations when the laser frequency is scanned across the cavity resonance. As a result, the averaged spectrum of the cavity transmission (red curve) is significantly broader than the real cavity resonance. A correct description of the cavity transmission requires an appropriate inclusion of the optomechanical effect, which is developed in the following.

When the optical power is well below the oscillation threshold and the flapping mode of the double disk is dominantly driven by thermal fluctuations, the mechanical motion can be described by the following equation:

$$\frac{d^2x}{dt^2} + \Gamma_m \frac{dx}{dt} + \Omega_m^2 x = \frac{F_T(t)}{m_x}, \tag{S11}$$

where Ω_m, Γ_m, and m_x are the resonance frequency, damping constant, and effective mass of the flapping mode, respectively. F_T is the Langevin force driving the mechanical Brownian motion, a Markovin process with the following correlation function:

$$\langle F_T(t) F_T(t+\tau) \rangle = 2 m_x \Gamma_m k_B T \delta(\tau), \tag{S12}$$

where T is the temperature and k_B is Boltzmann's constant. It can be shown easily from Eqs. (S11) and (S12) that the Brownian motion of the flapping mode is also a Markovin process with a spectral correlation given by $\langle \widetilde{x}(\Omega_1)\widetilde{x}^*(\Omega_2)\rangle = 2\pi S_x(\Omega_1)\delta(\Omega_1-\Omega_2)$, where $\widetilde{x}(\Omega)$ is the Fourier transform of the mechanical displacement $x(t)$ defined as $\widetilde{x}(\Omega) = \int_{-\infty}^{+\infty} x(t)e^{i\Omega t}dt$, and $S_x(\Omega)$ is the spectral intensity for the thermal mechanical displacement with the following form:

$$S_x(\Omega) = \frac{2\Gamma_m k_B T/m_x}{(\Omega_m^2-\Omega^2)^2+(\Omega\Gamma_m)^2}. \tag{S13}$$

The time correlation of the mechanical displacement is thus given by

$$\langle x(t)x(t+\tau)\rangle = \frac{1}{2\pi}\int_{-\infty}^{+\infty} S_x(\Omega)e^{-i\Omega\tau}d\tau \equiv \langle x^2\rangle\rho(\tau) \approx \langle x^2\rangle e^{-\Gamma_m|\tau|/2}\cos\Omega_m\tau, \tag{S14}$$

where $\langle x^2\rangle = k_B T/(m_x\Omega_m^2)$ is the variance of the thermal mechanical displacement and $\rho(\tau)$ is the normalized autocorrelation function for the mechanical displacement.

To be general, we consider a doublet resonance in which two optical fields, one forward and the other backward propagating, circulate inside the microcavity and couple via Rayleigh scattering from the surface roughness. The optical fields inside the cavity satisfy the following equations:

$$\frac{da_f}{dt} = (i\Delta_0-\kappa/2-ig_{\mathrm{OM}}x)a_f + i\eta a_b + i\sqrt{\kappa_e}A_{in}, \tag{S15}$$

$$\frac{da_b}{dt} = (i\Delta_0-\kappa/2-ig_{\mathrm{OM}}x)a_b + i\eta a_f, \tag{S16}$$

where a_f and a_b are the forward and backward whispering-gallery modes (WGMs), normalized such that $U_j = |a_j|^2$ $(j=f,b)$ represents the mode energy. A_{in} is the input optical wave, normalized such that $P_{in} = |A_{in}|^2$ represents the input power. κ is the photon decay rate for the loaded cavity, and κ_e is the photon escape rate associated with the external coupling. $\Delta_0 = \omega-\omega_0$ is the frequency detuning from the input wave to the cavity resonance and η is the mode coupling coefficient. In the case of a continuous-wave input, Eqs. (S15) and (S16) provide a formal solution of the forward WGM:

$$a_f(t) = i\sqrt{\kappa_e}A_{in}\int_0^{+\infty}\cos(\eta\tau)f(\tau)e^{-ig_{\mathrm{OM}}\int_0^\tau x(t-\tau')d\tau'}d\tau, \tag{S17}$$

where $f(\tau)\equiv e^{(i\Delta_0-\kappa/2)\tau}$ represents the cavity response. Using Eq. (S14), we find that the statistically averaged intracavity field is given as:

$$\langle a_f(t)\rangle = i\sqrt{\kappa_e}A_{in}\int_0^{+\infty}\cos(\eta\tau)f(\tau)e^{-\frac{\varepsilon}{2}h(\tau)}d\tau, \tag{S18}$$

where $\varepsilon \equiv g_{\rm OM}^2\langle x^2\rangle$ and $h(\tau)$ is defined as

$$h(\tau) \equiv \iint_0^{\tau} \rho(\tau_1-\tau_2)d\tau_1 d\tau_2. \tag{S19}$$

Similarly, we can find the averaged energy for the forward WGM as:

$$\begin{aligned}\langle U_f(t)\rangle &= \kappa_e P_{in}\iint_0^{+\infty} f(\tau_1)f^*(\tau_2)\cos(\eta\tau_1)\cos(\eta\tau_2)e^{-\frac{\varepsilon}{2}h(|\tau_1-\tau_2|)}d\tau_1 d\tau_2 \\ &= \frac{\kappa_e P_{in}}{2\kappa}\frac{\kappa-i\eta}{\kappa-2i\eta}\int_0^{+\infty} e^{-\frac{\varepsilon}{2}h(\tau)}\left[f_c(\tau)+f_s^*(\tau)\right]d\tau + c.c.,\end{aligned} \tag{S20}$$

where $f_j(\tau) \equiv e^{(i\Delta_j-\kappa/2)\tau}$ $(j=c,s)$, with $\Delta_c = \Delta_0+\eta$ and $\Delta_s = \Delta_0-\eta$. $c.c.$ denotes complex conjugate.

As the transmitted power from the double disk is given by

$$P_T(t) = P_{in} + \kappa_e U_f(t) + i\sqrt{\kappa_e}\left[A_{in}^* a_f(t) - A_{in}a_f^*(t)\right], \tag{S21}$$

the averaged cavity transmission, $\langle T\rangle \equiv \langle P_T\rangle/P_{in}$, thus takes the form

$$\langle T\rangle = 1-\frac{\kappa_e\kappa_i}{2\kappa}\left\{\left[1-\frac{i\eta\,\kappa_e}{\kappa_i(\kappa-2i\eta)}\right]\int_0^{+\infty} e^{-\frac{\varepsilon}{2}h(\tau)}\left[f_c(\tau)+f_s^*(\tau)\right]d\tau + c.c.\right\}. \tag{S22}$$

In the case of a singlet resonance, $\eta = 0$ and Eq. (S22) reduces to the simple form expression

$$\langle T\rangle = 1-\frac{\kappa_e\kappa_i}{\kappa}\int_0^{+\infty} e^{-\frac{\varepsilon}{2}h(\tau)}\left[f(\tau)+f^*(\tau)\right]d\tau. \tag{S23}$$

In the absence of opto-mechanical coupling, $g_{\rm OM} = 0$ and Eq. (S23) reduces to the conventional form of

$$T = 1-\frac{\kappa_e\kappa_i}{\Delta_0^2+(\kappa/2)^2}, \tag{S24}$$

as expected.

Using the theory developed above and fitting the experimental averaged cavity transmission spectrum, we obtain the optical Q factor of the resonance, as shown in Fig. S3(b) for Sample I. The same approach is used to describe the cavity transmission of Sample II, given in Fig. 3(a) of the main text.

IV. POWER SPECTRAL DENSITY OF THE CAVITY TRANSMISSION

Here we provide the derivations of the power spectral density of the cavity transmission in the presence of mechanical Brownian motion. We present two theories, one for the linear-perturbation regime when the optomechanical effect is small, the other a non-perturbation theory accurate for arbitrarily strong optomechanical effect.

A. The linear-perturbation theory

If the induced optomechanical perturbations are small, Eq. (S17) can be approximated as

$$a_f(t) \approx i\sqrt{\kappa_e}A_{in}\int_0^{+\infty}\cos(\eta\tau)f(\tau)\left[1-ig_{\rm OM}\int_0^{\tau}x(t-\tau')d\tau'\right]d\tau. \tag{S25}$$

In this case, the transmitted optical field can be written as $A_T(t)=A_{in}+i\sqrt{\kappa_e}a_f(t)\approx A_0+\delta A(t)$, where A_0 is the transmitted field in the absence of the optomechanical effect and δA is the induced perturbation. They take the following forms:

$$A_0 \;=\; A_{in}\left[1-\kappa_e\int_0^{+\infty}\cos(\eta\tau)f(\tau)d\tau\right]\equiv A_{in}\hat{A}_0, \tag{S26}$$

$$\delta A(t) \;=\; ig_{\rm OM}\kappa_e A_{in}\int_0^{+\infty}d\tau\cos(\eta\tau)f(\tau)\int_0^{\tau}x(t-\tau')d\tau'. \tag{S27}$$

The transmitted power then becomes $P(t)=|A_T(t)|^2\approx|A_0|^2+A_0^*\delta A(t)+A_0\delta A^*(t)$. It is easy to show that $\langle\delta A(t)\rangle=0$ and $\langle P_T(t)\rangle=|A_0|^2$. As a result, the power fluctuations, $\delta P(t)\equiv P_T(t)-\langle P_T(t)\rangle$, become

$$\delta P(t)\approx g_{\rm OM}P_{in}\int_0^{+\infty}d\tau u(\tau)\int_0^{\tau}x(t-\tau')d\tau', \tag{S28}$$

where $u(\tau)\equiv i\kappa_e\cos(\eta\tau)[\hat{A}_0^*f(\tau)-\hat{A}_0f^*(\tau)]$. By using Eq. (S14), we find the autocorrelation function for the power fluctuation to be

$$\langle\delta P(t)\delta P(t+t_0)\rangle\approx\varepsilon P_{in}^2\iint_0^{+\infty}d\tau_1d\tau_2u(\tau_1)u(\tau_2)\psi(t_0,\tau_1,\tau_2), \tag{S29}$$

where $\psi(t_0,\tau_1,\tau_2)$ is defined as

$$\psi(t_0,\tau_1,\tau_2)\equiv\int_0^{\tau_1}d\tau_1'\int_0^{\tau_2}d\tau_2'\rho(t_0+\tau_1'-\tau_2'). \tag{S30}$$

Taking the Fourier transform of Eq. (S29), we obtain the power spectral density $S_P(\Omega)$ of the cavity transmission to be

$$S_P(\Omega)\approx g_{\rm OM}^2P_{in}^2H(\Omega)S_x(\Omega), \tag{S31}$$

where $S_x(\Omega)$ is the spectral intensity of the mechanical displacement given in Eq. (S13) and $H(\Omega)$ is the cavity transfer function given by

$$H(\Omega)=\left|\frac{1}{\Omega}\int_0^{+\infty}u(\tau)(e^{i\Omega\tau}-1)d\tau\right|^2. \tag{S32}$$

In the case of a singlet resonance, the cavity transfer function takes the form:

$$H(\Omega)=\frac{\kappa_e^2}{\left[\Delta_0^2+(\kappa/2)^2\right]^2}\frac{4\Delta_0^2(\kappa_i^2+\Omega^2)}{\left[(\Delta_0+\Omega)^2+(\kappa/2)^2\right]\left[(\Delta_0-\Omega)^2+(\kappa/2)^2\right]}. \tag{S33}$$

In most cases, the photon decay rate inside the cavity is much larger than the mechanical damping rate, $\kappa \gg \Gamma_m$. For a specific mechanical mode at the frequency Ω_m, the cavity transfer function can be well approximated by $H(\Omega) \approx H(\Omega_m)$. In particular, in the sideband-unresolved regime, the cavity transfer function is given by a simple form of

$$H = \frac{4\kappa_e^2 \kappa_i^2 \Delta_0^2}{\left[\Delta_0^2 + (\kappa/2)^2\right]^4}. \tag{S34}$$

Therefore, Eq. (S31) shows clearly that, if the optomechanical effect is small, the power spectral density of the cavity transmission is directly proportional to the spectral intensity of the mechanical displacement.

B. The non-perturbation theory

The situation becomes quite complicated when the optomechanical effects are large. From Eq. (S21), the autocorrelation function for the power fluctuation of the cavity transmission, $\delta P(t) \equiv P_T(t) - \langle P_T \rangle$, is given by

$$\begin{aligned}
\langle \delta P(t_1) \delta P(t_2) \rangle &= \kappa_e^2 \langle U_{f1} U_{f2} \rangle - \kappa_e \langle \left(A_{in}^* a_{f1} - A_{in} a_{f1}^*\right) \left(A_{in}^* a_{f2} - A_{in} a_{f2}^*\right) \rangle \\
&+ i\kappa_e^{3/2} \left[\langle U_{f1} \left(A_{in}^* a_{f2} - A_{in} a_{f2}^*\right) \rangle + \langle U_{f2} \left(A_{in}^* a_{f1} - A_{in} a_{f1}^*\right) \rangle \right] \\
&- \left[\kappa_e \langle U_f \rangle + i\sqrt{\kappa_e} \left(A_{in}^* \langle a_f \rangle - A_{in} \langle a_f^* \rangle\right) \right]^2,
\end{aligned} \tag{S35}$$

where $U_{fj} = U_f(t_j)$ and $a_{fj} = a_f(t_j)$ $(j = 1, 2)$. Equation (S35) shows that the autocorrelation function involves various correlations between the intracavity energy and field, all of which can be found using Eqs. (S14) and (S17). For example, we can find the following correlation for the intracavity field:

$$\begin{aligned}
&\langle \left(A_{in}^* a_{f1} - A_{in} a_{f1}^*\right) \left(A_{in}^* a_{f2} - A_{in} a_{f2}^*\right) \rangle \\
&= -\kappa_e P_{in}^2 \iint_0^{+\infty} d\tau_1 d\tau_2 C_1 C_2 e^{-\frac{\varepsilon}{2}(h_1 + h_2)} \left[f_1 f_2 e^{-\varepsilon\psi} + f_1 f_2^* e^{\varepsilon\psi} + c.c. \right],
\end{aligned} \tag{S36}$$

where, in the integrand, $C_j = \cos(\eta\tau_j)$, $h_j = h(\tau_j)$, $f_j = f(\tau_j)$ (with $j = 1, 2$), and $\psi = \psi(t_2 - t_1, \tau_1, \tau_2)$. $h(\tau)$ and $\psi(t_2 - t_1, \tau_1, \tau_2)$ are given by Eqs. (S19) and (S30), respectively.

Equations (S19) and (S30) show that $h(\tau)$ and $\psi(t_2 - t_1, \tau_1, \tau_2)$ vary with time on time scales of $1/\Omega_m$ and $1/\Gamma_m$. However, in the sideband-unresolved regime, $\kappa \gg \Gamma_m$ and $\kappa \gg \Omega_m$. As the cavity response function $f(\tau)$ decays exponentially with time at a rate of $\kappa/2$, the integrand in

Eq. (S36) becomes negligible when $\tau_1 \gg 2/\kappa$ or $\tau_2 \gg 2/\kappa$. Therefore, $\psi(t_2-t_1,\tau_1,\tau_2)$ can be well approximated as

$$\begin{aligned}\psi(t_2-t_1,\tau_1,\tau_2) &= \frac{1}{2\pi\langle x^2\rangle}\int_{-\infty}^{+\infty}\frac{S_x(\Omega)}{\Omega^2}e^{-i\Omega(t_2-t_1)}\left(e^{-i\Omega\tau_1}-1\right)\left(e^{i\Omega\tau_2}-1\right)d\Omega \\ &\approx \frac{\tau_1\tau_2}{2\pi\langle x^2\rangle}\int_{-\infty}^{+\infty}S_x(\Omega)e^{-i\Omega(t_2-t_1)}d\Omega = \tau_1\tau_2\rho(t_2-t_1). \end{aligned} \tag{S37}$$

Similarly, $h(\tau)\approx\tau^2$, since $h(\tau)=\psi(0,\tau,\tau)$. Therefore, Eq. (S36) becomes

$$\left\langle\left(A_{in}^*a_{f1}-A_{in}a_{f1}^*\right)\left(A_{in}^*a_{f2}-A_{in}a_{f2}^*\right)\right\rangle \approx -\kappa_e P_{in}^2\Phi(\Delta t, C_1C_2), \tag{S38}$$

where $\Delta t = t_2-t_1$ and $\Phi(\Delta t, C_1C_2)$ is defined as

$$\Phi(\Delta t, C_1C_2) \equiv \iint_0^{+\infty} d\tau_1 d\tau_2 C_1C_2 e^{-\frac{\varepsilon}{2}\left(\tau_1^2+\tau_2^2\right)}\left[f_1f_2e^{-\varepsilon\tau_1\tau_2\rho}+f_1f_2^*e^{\varepsilon\tau_1\tau_2\rho}+c.c.\right], \tag{S39}$$

with $\rho=\rho(\Delta t)$. Following a similar approach, we can find the other correlation terms in Eq. (S35). Using these terms in Eq. (S35), we find that the autocorrelation function of the power fluctuations is given by

$$\langle\delta P(t_1)\delta P(t_2)\rangle \approx \kappa_e^2P_{in}^2\Phi(\Delta t,\sigma_1\sigma_2) - \left[\kappa_e\langle U_f\rangle + i\sqrt{\kappa_e}\left(A_{in}^*\langle a_f\rangle - A_{in}\langle a_f^*\rangle\right)\right]^2, \tag{S40}$$

where $\sigma_j=\sigma(\tau_j)$ $(j=1,2)$ and $\sigma(\tau)$ is defined as

$$\sigma(\tau) \equiv \left[1-\frac{\kappa_e(\kappa^2+2\eta^2)}{\kappa(\kappa^2+4\eta^2)}\right]\cos(\eta\tau)+\frac{\eta\kappa_e}{\kappa^2+4\eta^2}\sin(\eta\tau). \tag{S41}$$

Moreover, Eq. (S18) and (S20) show that, in the sideband-unresolved regime, $\langle a_f\rangle$ and $\langle U_f\rangle$ are well approximated by

$$\langle a_f(t)\rangle \approx i\sqrt{\kappa_e}A_{in}\int_0^{+\infty}\cos(\eta\tau)f(\tau)e^{-\frac{\varepsilon}{2}\tau^2}d\tau, \tag{S42}$$

$$\langle U_f(t)\rangle \approx \kappa_eP_{in}\iint_0^{+\infty}f(\tau_1)f^*(\tau_2)\cos(\eta\tau_1)\cos(\eta\tau_2)e^{-\frac{\varepsilon}{2}(\tau_1-\tau_2)^2}d\tau_1d\tau_2. \tag{S43}$$

Therefore, we obtain the final term in Eq. (S40) as

$$\kappa_e\langle U_f\rangle + i\sqrt{\kappa_e}\left(A_{in}^*\langle a_f\rangle - A_{in}\langle a_f^*\rangle\right) \approx -\kappa_eP_{in}\int_0^{+\infty}\sigma(\tau)\left[f(\tau)+f^*(\tau)\right]e^{-\frac{\varepsilon}{2}\tau^2}d\tau. \tag{S44}$$

Using this term in Eq. (S40), we obtain the final form for the autocorrelation of the power fluctuations:

$$\langle\delta P(t_1)\delta P(t_2)\rangle \approx \kappa_e^2P_{in}^2\left[\Phi(\Delta t,\sigma_1\sigma_2)-\Phi(\infty,\sigma_1\sigma_2)\right]. \tag{S45}$$

It can be further simplified if we notice that the exponential function $e^{\pm\varepsilon\tau_1\tau_2\rho(\Delta t)}$ in Eq. (S39) can be expanded in a Taylor series as

$$e^{\pm\varepsilon\tau_1\tau_2\rho(\Delta t)} = \sum_{n=0}^{+\infty} \frac{(\pm\varepsilon\tau_1\tau_2)^n}{n!}\rho^n(\Delta t). \tag{S46}$$

Substituting this expression into Eq. (S39) and using it in Eq. (S45), we obtain the autocorrelation function for the power fluctuation in the following form

$$\langle \delta P(t)\delta P(t+t_0)\rangle \approx \kappa_e^2 P_{in}^2 \sum_{n=1}^{+\infty} \frac{\varepsilon^n \rho^n(t_0)}{n!} |G_n^* + (-1)^n G_n|^2, \tag{S47}$$

where G_n is defined as

$$G_n \equiv \int_0^{+\infty} \tau^n \sigma(\tau) f(\tau) e^{-\frac{\varepsilon}{2}\tau^2} d\tau. \tag{S48}$$

In the case of a singlet resonance, $\eta = 0$ and $\sigma(\tau)$ simplifies considerably to $\sigma = \kappa_i/\kappa$. The autocorrelation function for the power fluctuation is still described by Eq. (S47).

In general, the power spectral density of the cavity transmission is given by the Fourier transform of Eq. (S47):

$$S_p(\Omega) = \kappa_e^2 P_{in}^2 \sum_{n=1}^{+\infty} \frac{\varepsilon^n S_n(\Omega)}{n!} |G_n^* + (-1)^n G_n|^2, \tag{S49}$$

where $S_n(\Omega)$ is defined as

$$S_n(\Omega) = \int_{-\infty}^{+\infty} \rho^n(\tau) e^{i\Omega\tau} d\tau. \tag{S50}$$

Eq. (S13) shows that the spectral intensity of the mechanical displacement can be approximated by a Lorentzian function, resulting in an approximated $\rho(\tau)$ given as $\rho(\tau) \approx e^{-\Gamma_m|\tau|/2}\cos\Omega_m\tau$ [see Eq. (S14)]. As a result, Eq. (S50) becomes

$$S_n(\Omega) \approx \frac{1}{2^n} \sum_{k=0}^{n} \frac{n!}{k!(n-k)!} \frac{n\Gamma_m}{(n\Gamma_m/2)^2 + [(2k-n)\Omega_m + \Omega]^2}. \tag{S51}$$

Combining Eq. (S49) and (S51), we can see that, if the optomechanical coupling is significant, the thermal mechanical motion creates spectral components around the harmonics of the mechanical frequency with broader linewidths. As shown clearly in Fig. 3(b) of the main text, the second harmonic is clearly visible. In particular, if the fundamental mechanical linewidth is broad, various frequency components on the power spectrum would smear out, producing a broadband spectral background, as shown in the top panel of Fig. 3(b) in the main text for Sample I. This phenomenon is similar to the random-field-induced spectral broadening in nuclear magnetic resonance [1] and atomic resonance fluorescence [2].

The theory developed in this section can be extended easily for the case with multiple mechanical frequencies. In this case, power spectrum only only exhibits harmonics of each mechanical frequency, but also their frequency sums and differences. As shown in the bottom panel of Fig. 3(b) of the main text, the frequency components near 0 MHz is the differential frequencies and those near 18-20 MHz are the second harmonics and sum frequencies.

V. NUMERICAL SIMULATION OF OPTOMECHANICAL OSCILLATIONS

The optomechanical oscillations are simulated through the following coupled equations governing the intracavity optical field and mechanical motions, respectively:

$$\frac{da}{dt} = (i\Delta_0 - \frac{\kappa}{2} - ig_{\mathrm{OM}}x)a + i\sqrt{\kappa_e}A_{in}, \tag{S52}$$

$$\frac{d^2x}{dt^2} + \Gamma_m\frac{dx}{dt} + \Omega_m^2 x = \frac{F_T(t)}{m_x} + \frac{F_o(t)}{m_x}, \tag{S53}$$

where we have counted in both the thermal Langevin force F_T and the optical gradient force $F_o = -\frac{g_{\mathrm{OM}}|a|^2}{\omega_0}$ for actuating mechanical motions.

VI. MAPPING THE THRESHOLD DETUNING

Figure S4 shows an example of the cavity transmission of Sample I. The mechanical flapping mode starts to oscillate when the input laser frequency is scanned across a certain detuning. Within this detuning value, the same magnitude of optomechanical oscillation is excited over a broad range of laser blue detuning. The intense transmission oscillations cover the entire coupling depth, leaving an abrupt kink on the transmission spectrum. The coupling depth at the kink point, ΔT_{th}, corresponds to the threshold coupling at the given power level, from which we can obtain the threshold frequency detuning Δ_{th}.

VII. FLAPPING MODES WITH VARIOUS AZIMUTHAL MODE NUMBERS

Because of the extremely short round-trip time of the cavity mode, the optical wave is sensitive only to the variations of averaged disk spacing around the whole disk. As a result, the optomechanical coupling for the fundamental flapping mode, which has flapping amplitude uniformly distributed around the disk perimeter, is maximum, but is nearly zero for flapping mode with

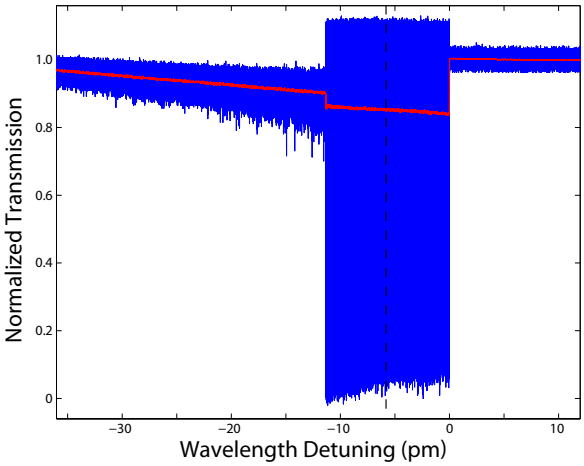

FIG. S4: Scan of the cavity transmission of Sample I at an input power of 0.76 mW, with the instantaneous and averaged signals shown in blue and red, respectively. The dashed line indicated the laser frequency detuning used to record the time-dependent cavity transmission given in Fig. 3(d) in the main text.

high-order azimuthal mode numbers. However, due to the asymmetry in practical devices, the net variations of averaged disk spacing induced by the high-order flapping modes (with azimuthal mode number ≥ 1) is not zero, and their thermal motion is visible in the transmission power spectrum. In general, their optomechanical coupling is weak and does not provide efficient dynamic back action.

VIII. COOLING OF THERMAL MECHANICAL MOTION

A. Spectral intensity of optically damped thermal mechanical motion

In general, the optomechanical effect is governed by Eqs. (S52) and (S53). However, the optomechanical effect during mechanical cooling is well described by linear perturbation theory since the thermal mechanical motions are significantly suppressed. The intracavity field can thus be approximated as $a(t) \approx a_0(t) + \delta a(t)$, where a_0 is the cavity field in the absence of optomechanical coupling and δa is the perturbation induced by the thermal mechanical motions. From Eq. (S52), they are found to satisfy the following equations:

$$\frac{da_0}{dt} = (i\Delta_0 - \kappa/2)a_0 + i\sqrt{\kappa_e}A_{in}, \tag{S54}$$

$$\frac{d\delta a}{dt} = (i\Delta_0 - \kappa/2)\delta a - ig_{\mathrm{OM}}xa_0. \tag{S55}$$

In the case of a continuous-wave input, Eq. (S54) gives a steady-state value given as:

$$a_0 = \frac{i\sqrt{\kappa_e}A_{in}}{\kappa/2 - i\Delta_0}, \tag{S56}$$

and Eq. (S55) provides the spectral response for the perturbed field amplitude,

$$\delta\widetilde{a}(\Omega) = \frac{ig_{\mathrm{OM}}a_0\widetilde{x}(\Omega)}{i(\Delta_0+\Omega) - \kappa/2}, \tag{S57}$$

where $\delta\widetilde{a}(\Omega)$ is the Fourier transform of $\delta a(t)$ defined as $\delta\widetilde{a}(\Omega) = \int_{-\infty}^{+\infty}\delta a(t)e^{i\Omega t}dt$. Similarly, $\widetilde{x}(\Omega)$ is the Fourier transform of $x(t)$.

The optical gradient force, $F_o = -\frac{g_{\mathrm{OM}}|a|^2}{\omega_0}$, is given by

$$F_o(t) = -\frac{g_{\mathrm{OM}}}{\omega_0}\left[|a_0|^2 + a_0^*\delta a(t) + a_0\delta a^*(t)\right]. \tag{S58}$$

The first term is a static term which only affects the equilibrium position of the mechanical motion, and can be removed simply by shifting the zero-point of the mechanical displacement to the new equilibrium position. Therefore, we neglect this term in the following discussion. The second and third terms provide the dynamic optomechanical coupling. From Eq. (S57), the gradient force is given by the following equation in the frequency domain:

$$\widetilde{F}_o(\Omega) = -\frac{2g_{\mathrm{OM}}^2|a_0|^2\Delta_0\widetilde{x}(\Omega)}{\omega_0}\frac{\Delta_0^2 - \Omega^2 + (\kappa/2)^2 + i\kappa\Omega}{[(\Delta_0+\Omega)^2 + (\kappa/2)^2]\,[(\Delta_0-\Omega)^2 + (\kappa/2)^2]}. \tag{S59}$$

As expected, the gradient force is linearly proportional to the thermal mechanical displacement.

Equation (S53) can be solved easily in the frequency domain, which becomes

$$(\Omega_m^2 - \Omega^2 - i\Gamma_m\Omega)\widetilde{x} = \frac{\widetilde{F}_T}{m_x} + \frac{\widetilde{F}_o}{m_x}. \tag{S60}$$

Equation (S60) together with (S59) provides the simple form for the thermal mechanical displacement,

$$\widetilde{x}(\Omega) = \frac{\widetilde{F}_T}{m_x}\frac{1}{(\Omega_m')^2 - \Omega^2 - i\Gamma_m'\Omega}, \tag{S61}$$

where Ω_m' and Γ_m' are defined as

$$\begin{aligned}
(\Omega_m')^2 &\equiv \Omega_m^2 + \frac{2g_{\mathrm{OM}}^2|a_0|^2\Delta_0}{m_x\omega_0}\frac{\Delta_0^2 - \Omega^2 + (\kappa/2)^2}{[(\Delta_0+\Omega)^2 + (\kappa/2)^2]\,[(\Delta_0-\Omega)^2 + (\kappa/2)^2]} \\
&\approx \Omega_m^2 + \frac{2g_{\mathrm{OM}}^2|a_0|^2\Delta_0}{m_x\omega_0}\frac{\Delta_0^2 - \Omega_m^2 + (\kappa/2)^2}{[(\Delta_0+\Omega_m)^2 + (\kappa/2)^2]\,[(\Delta_0-\Omega_m)^2 + (\kappa/2)^2]}, \qquad \text{(S62)} \\
\Gamma_m' &\equiv \Gamma_m - \frac{2g_{\mathrm{OM}}^2|a_0|^2\kappa\Delta_0}{m_x\omega_0}\frac{1}{[(\Delta_0+\Omega)^2 + (\kappa/2)^2]\,[(\Delta_0-\Omega)^2 + (\kappa/2)^2]} \\
&\approx \Gamma_m - \frac{2g_{\mathrm{OM}}^2|a_0|^2\kappa\Delta_0}{m_x\omega_0}\frac{1}{[(\Delta_0+\Omega_m)^2 + (\kappa/2)^2]\,[(\Delta_0-\Omega_m)^2 + (\kappa/2)^2]}. \qquad \text{(S63)}
\end{aligned}$$

Equations (S61)-(S63) show clearly that the primary effect of the optical gradient force on the mechanical motion is primarily to change its mechanical frequency (the so-called optical spring effect) and energy decay rate to the new values given by Eqs. (S62) and (S63). The efficiency of optomechanical control is determined by the figure of merit $g_{\rm OM}^2/m_x$. On the red detuned side, the optical wave damps the thermal mechanical motion and thus increases the energy decay rate. At the same time, the mechanical frequency is modified, decreasing with increased cavity energy in the sideband-unresolved regime.

Using Eqs. (S12) and (S61), we find that the spectral intensity of the thermal displacement is given by a form similar to Eq. (S13):

$$S_x(\Omega) = \frac{2\Gamma_m k_B T/m_x}{[(\Omega'_m)^2 - \Omega^2]^2 + (\Omega\Gamma'_m)^2}, \tag{S64}$$

which has a maximum value $S_x(\Omega'_m) = \frac{2\Gamma_m k_B T}{m_x(\Omega'_m\Gamma'_m)^2}$. The variance of the thermal mechanical displacement is equal to the area under the spectrum,

$$\langle(\delta x)^2\rangle = \frac{1}{2\pi}\int_{-\infty}^{+\infty} S_x(\Omega)d\Omega = \frac{k_B T\Gamma_m}{m_x(\Omega'_m)^2\Gamma'_m}. \tag{S65}$$

Cooling the mechanical motion reduces the spectral magnitude and the variance of thermal displacement.

B. Effective temperature of the cooled mechanical mode

For a mechanical mode in thermal equilibrium, the effective temperature can be inferred from the thermal mechanical energy using the equipartition theorem:

$$k_B T_{\rm eff} = m_x(\Omega'_m)^2\langle(\delta x)^2\rangle. \tag{S66}$$

The area under the displacement spectrum thus provides an accurate measure of the effective temperature. In practice, fluctuations on the laser frequency detuning may cause the mechanical frequency and damping rate to fluctuate over a certain small range [Eq. (S62) and (S63)], with a probability density function of $p(\Omega'_m)$. As a result, the experimentally recorded displacement spectrum is given by the averaged spectrum

$$\overline{S}_x(\Omega) = \int S_x(\Omega)p(\Omega'_m)d\Omega'_m, \tag{S67}$$

where $S_x(\Omega)$ is given by Eq. (S64) and we have assumed $\int p(\Omega'_m)d\Omega'_m = 1$. The experimentally measured spectral area is thus

$$\frac{1}{2\pi}\int_{-\infty}^{+\infty}\overline{S}_x(\Omega)d\Omega = \int \langle(\delta x)^2\rangle p(\Omega'_m)d\Omega'_m \equiv \overline{\langle(\delta x)^2\rangle}. \tag{S68}$$

Therefore, the integrated spectral area obtained from the experimental spectrum is the averaged variance of thermal mechanical displacement, from which, according to the equipartition theorem, we obtain the effective average temperature

$$k_B\overline{T}_{\text{eff}} = m_x(\overline{\Omega}'_m)^2\overline{\langle(\delta x)^2\rangle}, \tag{S69}$$

where $\overline{\Omega}'_m \equiv \int \Omega'_m p(\Omega'_m)d\Omega'_m$ is the center frequency of the measured displacement spectrum $\overline{S}_x(\Omega)$. Compared with the room temperature, the effective temperature is thus given by

$$\frac{\overline{T}_{\text{eff}}}{T_0} = \frac{(\overline{\Omega}'_m)^2\overline{\langle(\delta x)^2\rangle}}{\overline{\Omega}_m^2\langle(\delta x)^2\rangle_0}, \tag{S70}$$

where $\langle(\delta x)^2\rangle_0$ is the displacement variance at room temperature, given by the spectral area at T_0.

---

[1] R. Kubo, "A stochastic theory of line shape," in *Advances in Chemical Physics vol. 15*, K. E. Shuler Ed. (John Wiley & Sons, New York, 1969).

[2] H. J. Kimble and L. Mandel, "Resonance fluorescence with excitation of finite bandwidth," Phys. Rev. A 15, 689 (1977).